

NON-PARAMETRIC DARK ENERGY RECONSTRUCTION USING THE TOMOGRAPHIC ALCOCK-PACZYNSKI TEST

ZHENYU ZHANG,¹ GAN GU,¹ XIAOMA WANG,¹ YUN-HE LI,² CRISTIANO G. SABIU,³ HYUNBAE PARK,⁴ HAITAO MIAO,¹
XIAOLIN LUO,¹ FENG FANG,¹ AND XIAO-DONG LI¹

¹*School of Physics and Astronomy, Sun Yat-Sen University, Guangzhou 510297, P.R.China*

²*Department of Physics, College of Sciences, Northeastern University, Shenyang 110004, China*

³*Department of Astronomy, Yonsei University, Seoul, Korea*

⁴*Kavli Institute for the Physics and Mathematics of the Universe, University of Tokyo, Chiba 277-8582, Japan*

(Received November 6, 2017; Revised November 27, 2017; Accepted May 10, 2019)

Submitted to ApJ

ABSTRACT

The tomographic Alcock-Paczynski (AP) method can result in tight cosmological constraints by using small and intermediate clustering scales of the large scale structure (LSS) of the galaxy distribution. By focusing on the redshift dependence, the AP distortion can be distinguished from the distortions produced by the redshift space distortions (RSD). In this work, we combine the tomographic AP method with other recent observational datasets of SNIa+BAO+CMB+ H_0 to reconstruct the dark energy equation-of-state w in a non-parametric form. The result favors a dynamical DE at $z \lesssim 1$, and shows a mild deviation ($\lesssim 2\sigma$) from $w = -1$ at $z = 0.5 - 0.7$. We find the addition of the AP method improves the low redshift ($z \lesssim 0.7$) constraint by $\sim 50\%$.

Keywords: large-scale structure of Universe — dark energy — cosmological parameters

arXiv:1902.09794v3 [astro-ph.CO] 9 May 2019

1. INTRODUCTION

The late-time accelerated expansion of the Universe (Riess et al. 1998; Perlmutter et al. 1999) implies either the existence of “dark energy” or the breakdown of general relativity on cosmological scales. The theoretical origin and observational measurements of cosmic acceleration, although have attracted tremendous attention, are still far from being well explained or accurately measured (Weinberg 1989; Li et al. 2011; Yoo & Watanabe 2012; Weinberg et al. 2013).

The Alcock-Paczynski (AP) test (Alcock & Paczynski 1979) enables us to probe the angular diameter distance D_A and the Hubble factor H , which can be used to place constraints on cosmological parameters. Under a certain cosmological model, the radial and tangential sizes of some distant objects or structures take the forms of $\Delta r_{\parallel} = \frac{c}{H(z)}\Delta z$ and $\Delta r_{\perp} = (1+z)D_A(z)\Delta\theta$, where Δz , $\Delta\theta$ are their redshift span and angular size, respectively. Thus, if incorrect cosmological models are assumed for transforming redshifts into comoving distances, the wrongly estimated Δr_{\parallel} and Δr_{\perp} induce a geometric distortion, known as the AP distortion. Statistical methods which probe and quantify the AP distortion has been developed and applied to a number of galaxy redshift surveys to constrain the cosmological parameters (Ryden 1995; Ballinger Peacock & Heavens 1996; Matsubara & Suto 1996; Outram et al. 2004; Blake et al. 2011; Lavaux & Wandelt 2012; Alam et al. 2016; Mao et al. 2016; Doogesh et al. 2018).

Recently, a novel tomographic AP method based on the redshift evolution of the AP distortion has achieved significantly strong constraints on the cosmic expansion history parameters (Park & Kim 2010; Li et al. 2014, 2015, 2016). The method focuses on the redshift dependence to differentiate the AP effect from the distortions produced by the redshift space distortions (RSD), and has proved to be successful in dealing with galaxy clustering on relatively small scales. Li et al. (2016) firstly applied the method to the SDSS (Sloan Digital Sky Survey) BOSS (Baryon Oscillation Spectroscopic Survey) DR12 galaxies, and achieves $\sim 35\%$ improvements in the constraints on Ω_m and w when combining the method with external datasets of the Cosmic Microwave Background (CMB), type Ia supernovae (SNIa), baryon acoustic oscillations (BAO), and the H_0 .

In this work we aim to study how the tomographic AP method can be optimised to aid in measuring and characterising dark energy. The non-parametric strategy is particularly suitable for constraining functions whose forms are not clearly known from the theoretical aspect (Marco Raveri 2019). We apply the method to reconstruct the dark energy equation-of-state $w(z)$,

using the non-parametric approach developed in Crittenden et al. (2009, 2012); Zhao et al. (2012), which has the advantage of not assuming any *ad hoc* form of w . In a recent work Zhao, G.-B. et al. (2017) use this method to reconstruct w from 16 observational datasets, and claim a 3.5σ significance level in preference of a dynamical dark energy. It would be interesting to see what the results would be if the tomographic AP method is used to reconstruct w , and whether the reconstructed w is consistent with the results of Zhao, G.-B. et al. (2017).

The brief outline of this paper is as follows. In §2 we outline the tomographic AP method and how we practically implement the non-parametric modelling of $w(z)$. In §3 we present the results of our analysis in combination with other datasets. We conclude in §4.

2. METHODOLOGY

In pursuit of reconstructing DE in a model-independent manner, we adopt the non-parametric method of w (Crittenden et al. 2009; Zhao et al. 2012) without choosing any particular parameterization. To start, w is parameterized in terms of its values at discrete steps in the scale factor a . Fitting a large number of uncorrelated bins would lead to extremely large uncertainties and, in fact, would prevent the Monte Carlo Markov Chains (MCMC) from converging due to the large number of degenerate directions in the parameter space. On the other hand, fitting only a few bins usually lead to an unphysical discrete distribution of w and significantly bias the result. The solution is to introduce a prior covariance among a large number of bins based on a phenomenological two-point function,

$$\xi_w(|a - a'|) \equiv \langle [w(a) - w^{\text{fid}}(a)][w(a') - w^{\text{fid}}(a')] \rangle, \quad (1)$$

which is chosen as the form of (Crittenden et al. 2009),

$$\xi_{\text{CPZ}}(\delta a) = \xi_w(a=0)/[1 + (\delta a/a_c)^2], \quad (2)$$

where $\delta a \equiv |a - a'|$. Clearly, a_c describes the typical smoothing scale, and $\xi_w(0)$ is the normalization factor determined by the expected variance of the mean of the w 's, σ_w^2 . The ‘floating’ fiducial is defined as the local average,

$$w_i^{\text{fid}} = \sum_{|a_j - a_i| \leq a_c} w_j^{\text{true}}/N_j, \quad (3)$$

where N_j is the number of neighbouring bins lying around the i -th bin within the smoothing scale.

In practice, one should set the priors to conduct the analysis. A very weak prior (i.e., small a_c or large σ_w^2) can match the true model on average (i.e., unbiased), but will result in a noisy reconstruction. A stronger prior reduces the variance but pulls the reconstructed

results towards the peak of the prior. In this paper, we use the “weak prior” $a_c = 0.06$, $\sigma_{\bar{w}} = 0.04$, the prior which was also adopted in [Zhao et al. \(2012\)](#). The tests performed in [Crittenden et al. \(2009\)](#) shown that the results are largely independent of the choice of the correlation function. Also, [Crittenden et al. \(2012\)](#) has showed that a stronger prior $\sigma_{\bar{w}} = 0.02$ is already enough for reconstructing a range of models without introducing a sizeable bias.

We parametrize w in terms of its values at N points in a , i.e.,

$$w_i = w(a_i), \quad i = 1, 2, \dots, N. \quad (4)$$

In this analysis we choose $N = 30$, where the first 29 bins are uniform in $a \in [0.286, 1]$, corresponding to $z \in [0, 2.5]$, and the last bin covers the wide range of $z \in [2.5, 1100]$. Given the binning scheme, together with the covariance matrix \mathbf{C} given by Equation 2, it is straightforward to write down prior following the Gaussian form PDF

$$\mathcal{P}_{\text{prior}}(\mathbf{w}) \propto \exp\left(-\frac{1}{2}(\mathbf{w} - \mathbf{w}^{\text{fid}})\mathbf{C}^{-1}(\mathbf{w} - \mathbf{w}^{\text{fid}})\right). \quad (5)$$

Effectively, the prior results in a new contribution to the total likelihood of the model given the datasets D ,

$$\mathcal{P}(\mathbf{w}|\mathbf{D}) \propto \mathcal{P}(\mathbf{D}|\mathbf{w}) \times \mathcal{P}_{\text{prior}}(\mathbf{w}), \quad (6)$$

thus penalizes those models who are less smooth.

The method is then applied to a joint dataset of recent cosmological observations including the CMB temperature and polarization anisotropies measured by full-mission Planck ([Ade et al. 2015](#)), the “JLA” SNIa sample ([Betoule et al. 2014](#)), a Hubble Space Telescope measurement of $H_0 = 70.6 \pm 3.3$ km/s/Mpc ([Riess et al. 2011](#); [Efstathiou 2014](#)), and the BAO distance priors measured from 6dFGS ([Beutler et al. 2011](#)), SDSS MGS ([Ross et al. 2015](#)), and the SDSS-III BOSS DR11 anisotropic measurements ([Anderson et al. 2013](#)), as was also adopted in [Li et al. \(2016, 2018\)](#).

These datasets are then combined with the AP likelihood of SDSS-III BOSS DR12 galaxies ([Li et al. 2016, 2018](#)), for which we evaluate the redshift evolution of LSS distortion induced by wrong cosmological parameters via the anisotropic correlation function,

$$\delta\hat{\xi}_{\Delta_s}(z_i, z_j, \mu) \equiv \hat{\xi}_{\Delta_s}(z_i, \mu) - \hat{\xi}_{\Delta_s}(z_j, \mu). \quad (7)$$

$\xi_{\Delta_s}(z_i, \mu)$ is the integrated correlation function which captures the information of LSS distortion within the clustering scales one were interested in,

$$\xi_{\Delta_s}(\mu) \equiv \int_{s_{\text{min}}=6 \text{ h}^{-1} \text{ Mpc}}^{s_{\text{max}}=40 \text{ h}^{-1} \text{ Mpc}} \xi(s, \mu) ds. \quad (8)$$

It was then normalized to remove the uncertainty from clustering magnitude and the galaxy bias,

$$\hat{\xi}_{\Delta_s}(\mu) \equiv \frac{\xi_{\Delta_s}(\mu)}{\int_0^{\mu_{\text{max}}} \xi_{\Delta_s}(\mu) d\mu}. \quad (9)$$

As described in Equation 7, the difference between $\hat{\xi}_{\Delta_s}(\mu)$ measured at two different redshifts z_i, z_j characterizes the amount of the redshift evolution of LSS distortion. SDSS DR12 has 361 759 LOWZ galaxies at $0.15 < z < 0.43$, and 771 567 CMASS galaxies at $0.43 < z < 0.693$. We split these galaxies into six, non-overlapping redshift bins of $0.150 < z_1 < 0.274 < z_2 < 0.351 < z_3 < 0.430 < z_4 < 0.511 < z_5 < 0.572 < z_6 < 0.693$ ¹ ([Li et al. 2016](#)).

[Li et al. \(2014, 2015\)](#) demonstrated that $\delta\hat{\xi}_{\Delta_s}(z_i, z_j, \mu)$ is dominated by the AP distortion while being rather insensitive to the RSD distortion, enabling us to avoid the large contamination from the latter and probe the AP distortion information on relative small clustering scales.

The only difference in our treatment from [Li et al. \(2016\)](#) is that here we slightly improve the method and adopt a “full-covariance matrix” likelihood

$$\mathcal{P}_{\text{AP}}(\mathbf{w}|\mathbf{D}) \propto \exp\left(-\frac{1}{2} \theta_{\text{AP}} \mathbf{C}_{\text{AP}}^{-1} \theta_{\text{AP}}\right), \quad (10)$$

where the vector

$$\theta_{\text{AP}} = \left[\hat{\xi}_{\Delta_s}(z_2, z_1, \mu_j), \hat{\xi}_{\Delta_s}(z_3, z_2, \mu_j), \dots, \hat{\xi}_{\Delta_s}(z_6, z_5, \mu_j)\right] \quad (11)$$

summarizes the redshift evolution among the six redshift bins into its $5 \times n_\mu$ components (n_μ is the number of binning in ξ_{Δ_s}). The covariance matrix \mathbf{C}_{AP} is estimated using the 2,000 MultiDark-Patchy mocks ([Kitaura et al. 2015](#)). Compared with [Li et al. \(2016\)](#), where the 1st redshift bin is taken as the reference, this current approach includes the statistical uncertainties in the system and avoids the particular dependence on which specific redshift bin is chosen as the reference.

This improved methodology was presented in [Li et al. \(2019\)](#), where the authors detailedly explained how the multi-redshifts correlation is included, and how it affects the constraints on the various cosmological parameters.

3. RESULTS

The derived constraints on w as a function of redshift are plotted in Figure 1. The red solid

¹ The boundaries are determined so that, for LOWZ and CMASS samples, the number of galaxies are same in each bin, respectively.

lines represent the 68.3% CL constraints based on Planck+SNIa+BAO+ H_0 , while the AP-added results are plotted in blue filled ².

The reconstructed $w(z)$ from Planck+SNIa+BAO+ H_0 ³ is fully consistent with the cosmological constant; the $w = -1$ line lies within the 68.3% CL region. In the plotted redshift range ($0 < z < 2.5$), the upper bound of w is constrained to $\lesssim -0.8$, while the lower bound varies from -1.3 at $z = 0$ to -2.0 at $z \gtrsim 2$, dependent on the redshift. The best constrained epoch lies around $z = 0.2$. These features are consistent with the previous results presented in the literature using a similar dataset (Zhao et al. 2017).

The constraints are much improved after adding AP to the combined dataset. At $z \lesssim 0.7$, i.e. the redshift range of the SDSS galaxies analyzed by the AP method, the uncertainty of $w(z)$ is reduced by $\sim 50\%$, reaching as small as 0.2. It then increases to 0.4-1.0 at higher redshift ($0.7 < z < 2.5$). This highlights the power of the AP method in constraining the properties of dark energy, which were shown in Li et al. (2016, 2018).

Although here the AP method only probes the expansion history information at $z \in (0.1, 0.7)$, it can still affect the high redshift constraints. At $0.7 \lesssim z \lesssim 1.0$, the constraints are tightened by the correlated prior of $w(z)$. At higher redshift, the error bars are less affected, but the values of w are shifted to more negative regions. This is due to the combination of AP and CMB data. Effectively, the CMB data constrain the $w(z)$ in a manner of the “shift parameter” $R \equiv \sqrt{\Omega_m} H_0 (1+z_*) D_A(z_*)$ (Bond et al. 1997), which constrains the integration of $1/H(z)$ in the range of $z \approx 0 - 1100$. So if the constraints on $z \lesssim 1.0$ are changed, the $z \gtrsim 1.0$ parts are also altered, correspondingly.

The most interesting phenomenon from our studies is that the result indicates a mild discrepancy with a constant $w = -1$. At $0.5 \lesssim z \lesssim 0.7$, $w > -1$ is slightly favored ($\lesssim 2\sigma$). The statistical significance of this result is not large enough to claim a detection of deviation from a cosmological constant, however this may be readdressed in the near future as the constraining power will become

² The AP and BAO methods probe galaxy clustering on very different scales, so it is safe to assume they have no correlation and can be simply combined. In Zhang et al. (2018), the authors have computed the correlation coefficient of the anisotropic information in the clustering scales of AP and BAO methods in N-body simulations, and find it as small as -0.054 ± 0.034 .

³ Note that the SDSS DR11 anisotropic BAO measurements also contains the AP information on scales of $\sim 100h^{-1}$ Mpc, so it is a little inappropriate to use the abbreviations “BAO” and “AP” in the legend. Anyway, we still use them, and our “AP” only stands for the 6-40 h^{-1} Mpc tomographic AP measurements of SDSS DR12 galaxies.

much improved when combining tomographic AP with the upcoming experiments of DESI (Aghamousa et al. 2016) or EUCLID (Laureijs et al. 2011).

The results also slightly favor a dynamical behavior of DE. At $z = 0 - 0.5$, we find phantom-like dark energy $-1.2 \lesssim w \lesssim -1.0$, while at higher redshift $z = 0.5 - 0.7$ it becomes quintessence-like, $-1.0 \lesssim w \lesssim -0.6$. Theoretically, this is known as the quintom dark energy (Feng et al. 2005).

The advantage of the tomographic AP method is that, it makes use of the clustering information in a series of redshift bins (rather than compresses the whole sample into a single effective redshift). Thus, it is able to capture the dynamical behavior of dark energy within narrow ranges of Δz .

Our results are consistent with the $w(z)$ obtained in Li et al. (2018), where the authors used the Planck+SNIa+BAO+ H_0 +AP dataset to constrain the CPL parametrization $w = w_0 + w_a \frac{z}{1+z}$. They found 100% improvement in the DE figure-of-merit and a slight preference of dynamical dark energy. Benefitting from a more general form of a non-parametric $w(z)$, we are able to obtain more detailed features in the reconstruction.

To further validate the results, we did an input-output test on two MultiDark-Patchy realizations ⁴. We treat the mocks as the “real data” and apply the AP method to them. The constraints on $w(z)$ are plotted in Figure 3. The “true” cosmology of $w = -1$ are nicely recovered (deviation $\lesssim 1\sigma$). The size of error bars are ~ 1.5 times of the Planck+SNIa+BAO+ H_0 +AP constraints of Figure 1. This justifies the ability of the tomographic AP method in constraining the non-parametric dark energy equation of state.

Finally, we note that the results with and without AP are in good consistency with each other. This implies that the information obtained from the AP effect agrees well with the other probes. Since the clustering information probed by AP is independent from those probed by BAO (see the discussion in Zhang et al. (2018)), to some extent, in this analysis these two different LSS probes compliment and validate each other. This is also consistent with the results of Li et al. (2016), where we found the contour region constrained by AP consistently overlaps with those of SNIa, BAO and CMB.

4. CONCLUDING REMARKS

⁴ As a simple check we just did it on two realizations. Due to the many degrees of freedom the MCMC chains converge very slowly, making it rather difficult to perform this kind of test on a large number of mocks.

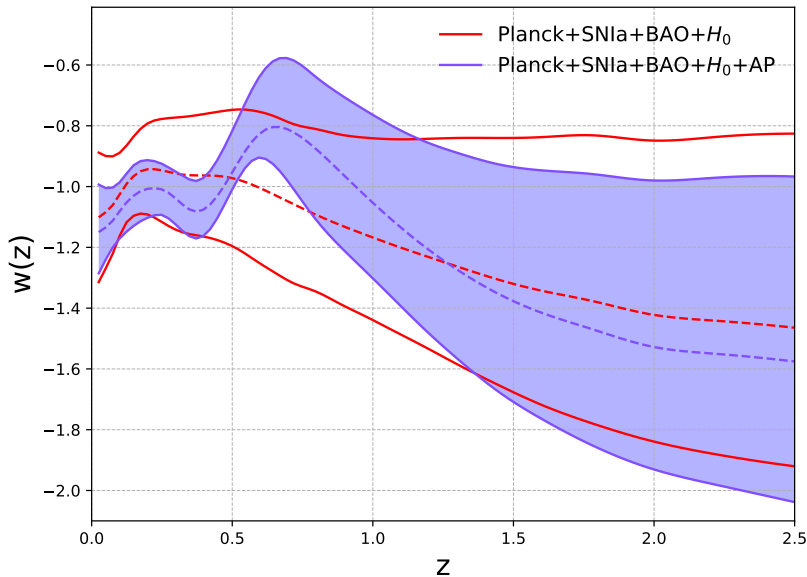


Figure 1. Derived redshift evolution of $w(z)$. The mean values and 68.3% CL regions are plotted. Adding the AP method tightens the constraints. Dynamical behavior of dark energy is mildly favored at $z \lesssim 0.7$.

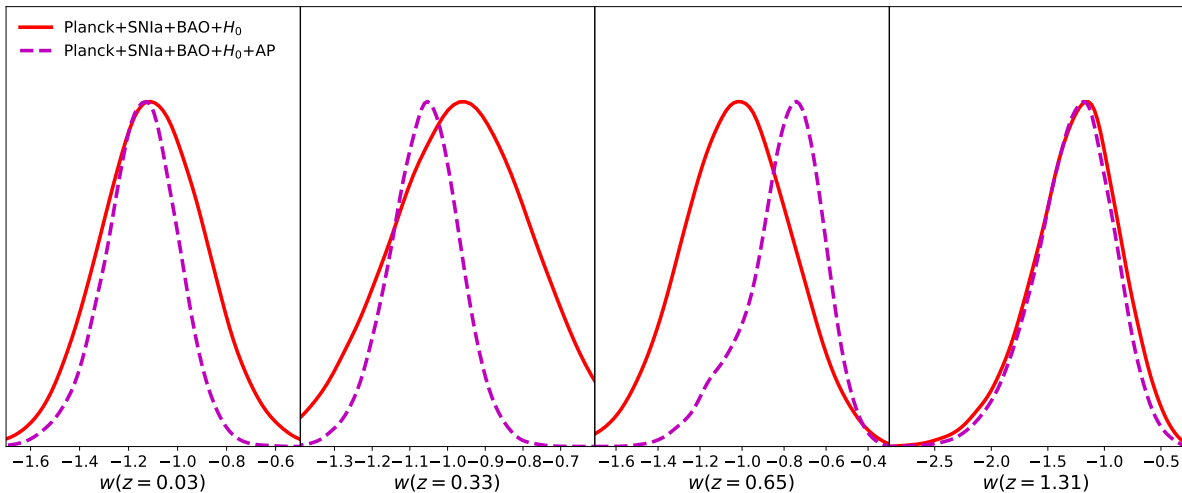


Figure 2. Likelihoods of $w(z = 0.03, 0.33, 0.65, 1.31)$ from Planck+SNla+BAO+ H_0 (red solid) and Planck+SNla+BAO+ H_0 +AP (purple dotted). The addition of AP improves the constraint at $z \lesssim 0.7$ by $\sim 50\%$.

In this work, we consider a very general, non-parametric form for the evolution of the dark energy equation-of-state, $w(z)$. We obtain cosmological constraints by combining our tomographic AP method with other recent observational datasets of SNIa+BAO+CMB+ H_0 . As a result, we find that the inclusion of AP improves the low redshift ($z < 0.7$) constraint by $\sim 50\%$. Moreover, our result favors a dynamical DE at $z \lesssim 1$, and shows a mild deviation ($\lesssim 2\sigma$) from $w = -1$ at $z = 0.5 - 0.7$.

We did not discuss the systematics of the AP method in details. This topic has been extensively studied in Li et al. (2016, 2018), where the authors found that for the current observations the systematical error is still much less than the statistical uncertainty.

We note that our constraint on $w(z)$ at $z \lesssim 0.7$ is the tightest within the current literature. The accuracy we achieved is as good as that of Zhao et al. (2017) in their “ALL16” combination, where they used

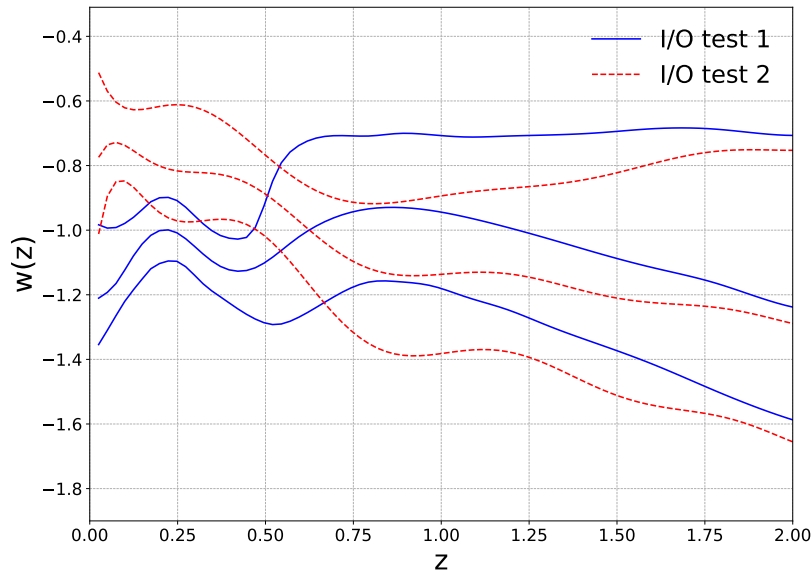


Figure 3. Input-output (I/O) test of the tomographic AP method, based on two MultiDark-Patchy realizations. Using the method the input cosmology $w = -1$ can be well recovered.

the Planck+SNIa+BAO+ H_0 datasets⁵, combined with the WiggleZ galaxy power spectra (Parkinson, D. et al. 2012), the CFHTLenS weak lensing shear angular power spectra Heymans, C. et al. (2013), the $H(z)$ measurement using relative age of old and passively evolving galaxies based on a cosmic chronometer approach (OHD; Moresco, M. et al. 2016), and the Ly α BAO measurements (Delubac, T. et al. 2015). In comparison, we use a much smaller number of datasets to achieve a similar low-redshift $w(z)$ constraint. This highlights the great power of our tomographic AP method using anisotropic clustering on small scales.

At higher redshift ($z \gtrsim 0.7$) our constraint is weaker than Zhao et al. (2017). It would be interesting to include more datasets (e.g. the ones used in their paper, the SDSS IV high redshift results, Zhao, et al. 2019) and then re-perform this analysis.

The dynamical behavior of dark energy at $z \approx 0.5-0.7$ has also been found in many other works (Zhao et al. 2017; Wang et al. 2018). Due to the limitation of current observations, it is not possible to claim a detection of dynamical dark energy at $> 5\sigma$ CL. We expect this can be achieved (or falsified) in the near future aided by more advanced LSS experiments, such as DESI (Aghamousa

et al. 2016), Euclid (Laureijs et al. 2011), and LSST (Marshall et al. 2017).

We thank Gong-bo Zhao, Yuting Wang and Qing-Guo Huang for helpful discussion. XDL acknowledges the supported from NSFC grant (No. 11803094). YHL acknowledges the support of the National Natural Science Foundation of China (Grant No. 11805031) and the Fundamental Research Funds for the Central Universities (Grant No. N170503009). CGS acknowledges financial support from the NRF (Grant No. 2017R1D1A1B03034900).

Based on observations obtained with Planck (<http://www.esa.int/Planck>), an ESA science mission with instruments and contributions directly funded by ESA Member States, NASA, and Canada.

Funding for SDSS-III has been provided by the Alfred P. Sloan Foundation, the Participating Institutions, the National Science Foundation, and the U.S. Department of Energy Office of Science. The SDSS-III web site is <http://www.sdss3.org>. SDSS-III is managed by the Astrophysical Research Consortium for the Participating Institutions of the SDSS-III Collaboration including the University of Arizona, the Brazilian Participation Group, Brookhaven National Laboratory, Carnegie Mellon University, University of Florida, the French Participation Group, the German Participation Group, Harvard University, the Instituto de Astrofísica de Canarias, the Michigan State/Notre Dame/JINA Partic-

⁵ Zhao et al. (2017) used the SDSS galaxy BAO measurements at nine effective redshifts, which are measurements at more redshift points than our adopted BAO dataset, and is expected to be more powerful in such a $w(z)$ reconstruction analysis.

ipation Group, Johns Hopkins University, Lawrence Berkeley National Laboratory, Max Planck Institute for Astrophysics, Max Planck Institute for Extraterrestrial Physics, New Mexico State University, New York Uni-

versity, Ohio State University, Pennsylvania State University, University of Portsmouth, Princeton University, the Spanish Participation Group, University of Tokyo, University of Utah, Vanderbilt University, University of Virginia, University of Washington, and Yale University.

REFERENCES

- Ade, P.A.R., Aghanim, N., & Arnaud, M., et al. arXiv:1502.01589
- Aghamousa, A., 2016, arXiv:1611.00036
- Alam, S., Ata, M., & Bailey, S., et al. 2016, submitted to MNRAS (arXiv:1607.03155)
- Alcock, C., & Paczynski, B. 1979, *Nature*, 281, 358 We did not discuss the systematics of the AP method in details.
- Anderson, L., Aubourg, É., & Bailey, S. et al. 2014, MNRAS, 441, 24
- Ballinger, W.E., Peacock, J.A., & Heavens, A.F. 1996, MNRAS, 282, 877
- Betoule, M., Kessler, R., & Guy, J., et al. 2014, *A&A*, 568, 32
- Beutler, F., Blake, C., & Colless, M., et al. 2011, MNRAS, 416, 3017
- Bond, J. R., Efstathiou, G., & Tegmark M. 1997, MNRAS, 291, L33
- Blake, C., Glazebrook, K., & Davis, T. M., 2011, MNRAS, 418, 1725
- Crittenden, R.G. et al. 2012, JCAP, 02, 048
- Crittenden, R. G., Pogosian, Li, & Zhao, G.-B., 2009. JCAP, 0912, 025
- Crittenden, R. G., Zhao, G.-B., & Pogosian, Li, et al. 2012. JCAP, 1202, 048
- Delubac, T. et al. 2015, *Astron. & Astrophys.* 574, A59
- Kodi Ramanah, D., Lavaux, G, Jasche, J., & Wandelt, B.D., et al. 2019, *A&A*, 621, A69
- Efstathiou, G. 2014, MNRAS, 440, 1138
- Feng, B., Wang., X. L., & Zhang, X. M., 2005. *Phys. Lett. B.*, 607, 35
- Heymans, C. et al. 2013, *Mon. Not. R. Astron. Soc.* 432, 24332453. 1303.1808.
- Kim, J., Park, C., L’Huillier, B., & Hong, S. E. 2015, JKAS, 48, 213
- Kitaura, F.S., Rodriguez-Torres, S., Chuang, C.-H., et al. arXiv:1509.06400
- Laureijs, R., Amiaux, J., & Arduini, S., et al. 2011, arXiv:1110.3193
- Lavaux, G., & Wandelt, B.D. 2012, *ApJ*, 754, 109
- Li, M., Li, X.-D., Wang, S., & Wang, Y. 2011, *Commun. Theor. Phys.*, 56, 525
- Li, X.-D., Park, C., Forero-Romero, J., & Kim, J. 2014, *ApJ*, 796, 137
- Li, X.-D., Park, C., Sabiu, C.G., & Kim, J. 2015, MNRAS, 450, 807
- Li, X.-D., Park, C., & Sabiu, C.G., et al. 2016, *ApJ*, 832, 103
- Li, X.-D., Sabiu, C.G., & Park, C., et al. 2018, *ApJ*, 856, 88
- Li, X.-D., Miao, H., & Wang, X., et al. 2019, submitted to *ApJ*, arXiv:1903.04757
- Mao, Q., Berlind, A.A., Scherrer, R.J., et al. 2016, submitted to *ApJ*
- Marco R., 2019, arXiv:1902.01366
- Marshall, Phil, Anguita, Timo, & Bianco, F. B., et al. 2017, arXiv:1708.04058
- Matsubara T., & Suto, Y. 1996, *ApJ*, 470, L1
- Moresco, M. et al. 2016, *J. Cosmol. Astropart. Phys.* 5, 014. 1601. 01701.
- Outram, P.J., Shanks, T., Boyle, B.J., Croom, S.M., Hoyle, F., Learing, N.S., Miller, L., & Smith, R.J. 2004, MNRAS, 348, 745
- Park, C., & Kim, Y.-R. 2010, *ApJL*, 715, L185
- Parkinson, D. et al. 2012, *Phys. Rev. D* 86, 103518. 1210.2130.
- Perlmutter, S., Aldering, G., & Goldhaber, G., et al. 1999, *ApJ*, 517, 565
- Riess, A.G., Filippenko, A.V., & Challis, P., et al. 1998, *AJ*, 116, 1009
- Riess, A.G., Macri, L., & Casertano, S., et al. 2011, *ApJ*, 730, 119
- Ross, A.J., Samushia, L., & Howlett, C., et al. 2015, MNRAS, 449, 835
- Ryden, B.S. 1995, *ApJ*, 452, 25
- Weinberg, S. 1989, *Reviews of Modern Physics*, 61, 1
- Weinberg, D.H, Mortonson, M.J., Eisenstein, D.J., et al. 2013, *Physics Reports*, 530, 87
- Wang, Y., Pogosian, L., Zhao, G.-B., & Zucca, A. 2018. accepted by *ApJL*
- Yoo, J., & Watanabe, Y. 2012, *International Journal of Modern Physics D*, 21, 1230002
- Zhang, X., Huang, Q.-G., & Li, X.-D. 2018. *Mon. Not. R. Astron. Soc.*, 483, 1655

Zhao, G.-B., Crittenden, R.-G., Pogossian, L., & Zhang, X,
2012. Phys. Rev. Lett., 109, 171301

Zhao, G.-B., Raveri, M., & Pogossian, L., et al. 2017, Nat.
Astron., 1, 627

Zhao, G.-B. et al. 2017, Mon. Not. R. Astron. Soc. 466, 762

Zhao, G.-B. et al. 2019, MNRAS, 482, 3497